Sensors and Actuators Reports 6 (2023) 100176

Contents lists available at ScienceDirect

Sensors and Actuators Reports

journal homepage: www.sciencedirect.com/journal/sensors-and-actuators-reports

# Electroanalytical Overview: The Electroanalytical Detection of Oxalate

Robert D. Crapnell, Prashanth S. Adarakatti, Craig E. Banks *

*Faculty of Science and Engineering, Manchester Metropolitan University, Chester Street, Manchester, M1 5GD, United Kingdom*

ARTICLE INFO

*Keywords:*
oxalate
sensing
electrochemistry
electroanalytical
sensor
hyperoxaluria

ABSTRACT

The sensing of oxalate within urine has been recognised as one of the most important determinations in the investigation of patients with hyperoxaluria. However, current approaches have reported expensive, time consuming, occasionally poor selectivity and are subject to large inaccuracies if great care is not exercised in the handling and measurement of samples. One approach is the use of electroanalytical sensors, which present rapid but highly selective and sensitive outputs, are economical and miniature providing portable sensing platforms to support on-site analysis. In this minireview, recent advances in the electroanalytical sensing of oxalate are presented, overviewing recent electrode configurations and real sample analysis; comparisons to other analytical methods are presented. Finally, the conclusions and future perspective of this field are described in brief.

## 1. Introduction to oxalate

Oxalate is an anion having the chemical formula $C_2O_4^{2-}$, which is a product of protein metabolism excreted by the kidneys. Oxalate is excreted from humans via urine, which can indicate kidney lesions, hyperoxaluria, renal failure, pancreatic insufficiency, and is useful in the management of urolithiasis [1–5]. Related to hyperoxaluria there are many issues that are oxalate-related disorders: 1) *primary hyperoxaluria,* which is a rare genetic disorder that leads to an overproduction of oxalate by the liver where excess oxalate cannot be excreted by the kidneys and accumulates in the body, leading to the formation of calcium oxalate crystals forming kidney stone (nephrolithiasis) [6,7]. These crystals can build up in the kidneys and urinary tract, resulting in recurrent kidney stones, kidney damage, and potentially kidney failure if left untreated; 2) *secondary hyperoxaluria*, unlike primary hyperoxaluria, secondary hyperoxaluria is not caused by a genetic mutation. Instead, it arises from certain medical conditions, medications, or dietary habits that increase the production or absorption of oxalate. For example, conditions such as ethylene glycol poisoning, vitamin $B_6$ deficiency, or excessive consumption of high-oxalate foods can contribute to secondary hyperoxaluria. The clinical measurement of oxalate levels is important for diagnosing and managing various conditions related to oxalate metabolism and accumulation. Oxalate levels can be measured in urine, blood, and sometimes other bodily fluids which is achieved via urinary oxalate measurement where stone analysis, imaging but more performed are blood and urinary analysis where it is reported that oxalate concentrations in urine should be less than $\leq$460 μM/24 hrs [8] but in terms of human blood, levels are typically 1 to 5 μM [9]. Additionally, the determination of oxalates within foods is important for the health of human society. Related to oxalate is oxalic acid, $H_2C_2O_4$, which is the simplest dicarboxylic acid and yet it is found in a plethora of plants, microorganisms and animals [10], but it reacts with chelator of cations and is often found as soluble sodium or potassium oxalate, or precipitated as insoluble calcium oxalate which it is reported that 70–80% of patients presenting with kidney stones [11].

Oxalate has been measured using fluorescence [12], microchip electrophoresis [13], luminescence [14], liquid chromatography – mass spectrophotometry [15], to name just a few. However, these approaches have been reported as time consuming, require pre-treatment, are expensive, occasionally have a poor selectivity, and are subject to large inaccuracies if great care is not exercised in the handling and measurement of samples and also they are unsuitable where mobility of the equipment is needed [16]. An authoritative review has been provided an analytical overview [9], but we wish to explore further into electrochemical approaches. Electrochemical sensors are devices that utilize electrochemical reactions to detect and measure the concentration of specific analytes within a sample. These sensors utilize electrochemical techniques to measure the concentration of target analytes by monitoring changes in electrical properties, such as current, potential, or impedance, at an electrode-electrolyte interface. Electrochemical sensors are widely used in various fields, including environmental monitoring, medical diagnostics, industrial processes, and consumer electronics, due to their high sensitivity, selectivity, and relatively simple operation. Developing cheap, easily miniaturised and portable

* Corresponding author.
*E-mail address:* c.banks@mmu.ac.uk (C.E. Banks).

https://doi.org/10.1016/j.snr.2023.100176
Received 15 July 2023; Received in revised form 17 August 2023; Accepted 18 September 2023
Available online 19 September 2023

electrochemical sensors often involves simplifying the design, using cost-effective materials, such as carbon, and optimizing manufacturing processes. In this minireview, we have focused upon the electroanalytical sensors for the measurement of oxalate providing a summary of this field and where research needs to be redirected.

## 2. Electrochemical based sensors for oxalate

Table 1 shows a range of electrochemical sensors that have been designed and developed for the measurement of oxalates. As noted above, we use the term oxalate throughout but within Table 1, we specify which analyte which was measured, *e.g.,* oxalate, $C_2O_4^{2-}$ or oxalic acid $H_2C_2O_4$. The first report using electrochemistry spans back to 1979, where Mayer and co-workers have reported upon the determination of oxalic acid in urine using high performance liquid chromatography with electrochemical detection using a wax-impregnated graphite electrode [17]. In their approach, human urine is acidified with HCl to pH 3 which it is heated to 60 degrees for 15 mins. After cooling to room temperature, the acidified urine was centrifugated, where the pH was modified to 4.5 and calcium chloride is added to precipitate oxalate ions. The precipitate is isolated, redissolved in dilute sulfuric acid and separated on a strong cation exchange column using an acetic acid-sodium acetate-tetrabutylammonium tetrafluoroborate mobile phase adjusted to pH 2.8 [17]. The electrochemical detector was set at +1.25 V where a linear dynamic range from 11.4 μM to 11.4 mM with a limit of detection (LoD) reported to be 1.1 μM. The authors demonstrated that this has merits while obtaining a percentage recovery for spiked urine samples was 97.8% with a relative standard deviation of 2.5% [17]. Fogg et al. [18] reported the use of flow through injection analysis (FIA) using a glassy carbon electrode that has been electrochemically pre-treated for the sensing of oxalic acid. The authors reported that sensitive but yet reproducible signal can only be obtained through a pre-treatment of + 1.75 V for 10 mins then at -1.0 V for 1 min within a phosphate buffer (pH 7) used as the eluent, which gives rise to well-shaped hydrodynamic voltammograms at the optimized potential of + 1.5 V; the authors demonstrated that the dynamic range of 0.01 – 0.71 μM is possible [18].

Shaidarova et al.[19] take a traditional approach via the use of palladium nanoparticles which were electrochemically deposited upon a carbon paste electrode. Carbon paste electrodes (CPE) have the attention as one of the most studied electroanalytical platforms due to their advantages which includes, chemical inertness, robustness, renewability, stable response, low ohmic resistance where surface passivation is eliminated by a modest and quick renewal of their surface [20,21]. The authors reported that the analytical signal was due to the electrochemical oxidation of palladium with the generation of catalytically active palladium (II) species oxidizing oxalate [19]:

$$H_2C_2O_4 + Pd(II) \rightarrow 2CO_2 + 2H^+ + Pd^0 \quad (1)$$

Interestingly, the authors found that as the dispersity of palladium nanoparticles electrodeposited on the CPE surface increased and their size diminished, the peak current of the catalytic oxidation of oxalic acid decreased. In contrast the increment of this current increased as compared to the limiting current of metal oxidation which was attributed due to an increase in the catalytic activity of the palladium metal. The authors reported that a linear range of $10^{-2}$ – $10^{-5}$ M is possible with a LoD stated as 20 μM. This has been further explored via palladium electrodeposited upon a glassy carbon (GC) electrode where they explored the effects of applied potential, scan rate, pH, palladium loading, Pd(II) bulk concentration, and the rotation speed of the electrode on the electrooxidation process of oxalic acid [22]. It was reported that the electrochemical oxidation of oxalate undergoes first a preliminary slow adsorption step:

$$Pd^0 + H_2C_2O_4 \leftrightarrow Pd(H_2C_2O_4)_{ads} \quad (2)$$

which then undergoes a fast concerted hydrogen abstraction mechanism:

$$Pd(H_2C_2O_4)ads \rightarrow Pd^0 + 2CO_2 + 2H^+ \quad (3)$$

Through the use of the rotating disc electrode, a diffusion coefficient was reported to be $2.5 \times 10^{-5}$ $cm^2$ $s^{-1}$. This was extended through liquid chromatography using the palladium modified glassy carbon electrode (GCE) [23], which gave a linear range from 0.2 - 1.2 μM and a LoD reported to be 0.15 μM. The effects of several interferents were explored: chloride, ascorbic acid, pyruvic acid, uric acid, sulfite, thiocyanate, glucose, BSA, SDS, glycine, urea and gluconic acid. It was reported that small interference effects were observed for ascorbic acid, pyruvic acid, uric acid, gluconic acid, sulfite, glucose, BSA, SDS, glycine, and urea where the amperometric signal of less than 5% were obtained, however, a significant interference effect for chloride and thiocyanate ions was observed: variations of +15% and −55% on the amperometric signal were obtained in presence of chloride (90 mM) and thiocyanate (80 μM), respectively. The diminution of the electroanalytical signal of in the presence of thiocyanate it is reported due to the stronger adsorption effects of this ion on the catalytic sites. The authors went on to analyse oxalic acid within human urine, reporting good recoveries (95-98%). In a similar approach, palladium modified with a polyvinylpyridine film supported upon a GCE has also been reported, which exhibited a linear range of $10^{-2}$ to $10^{-6}$ M [24]. Related to the use of CPEs, other work has reported upon the use of spongy osmium which proceeds via the following scheme: [25]

$$[O_SO_x.nH_2O]\text{-}e + OH^- \rightarrow [O_SO_xOH.nH_2O] \quad (4)$$

$$[O_SO_xOH.nH_2O] + 1/2C_2O_4^{2-} \rightarrow [O_SO_x.nH_2O] + CO_2 + OH^- \quad (5)$$

which exhibits electrocatalytic activity. This sensor was simply made through the addition of spongy osmium of 2 – 5 wt% into the carbon paste. This approach utilized FIA reported a linear range of 0.05 – 350 μM with a LoD of 10 nM [25]. While a reputable electroanalytical response, further work needs to be measurement within real samples and the real use of using a highly extremely toxic substance need questioning.

Associated to the use of use of metal nanoparticles, Fang et al. have reported upon a facile sensor that is fabricated via a one-step co-electrodeposition to produce platinum nanoparticles adhered with porous silica (porous-$SiO_2$-Pt NPs) [26]; please see Fig. 1 for an overview.

The porous-$SiO_2$-Pt NPs composite electrode comprises 10 – 15 nm diameter platinum nanoparticles which are adhered to porous silicon dioxide which are easily fabricated by taking a solution of ammonium hexafluorosilicate and chloroplatinic acid via electrochemical deposition by applying a cathode current for 5 mins. In this approach, hydrogen bubbles are formed which give rise to a porous surface. The composite electrode is shown to measure 0 to 45 μM with a LoD of 25 nM; see Fig. 1B and C. The sensor was explored towards interferents, namely: formic acid, acetate, glucose, tartaric acid, ascorbic acid, $Zn^{2+}$, $Cu^{2+}$, $Mg^{2+}$, $Mn^{2+}$, and $Fe^{2+}$ which showed no response indicated that the porous-$SiO_2$-Pt NPs have a specificity for oxalic acid. The sensor was explored to the sensing of oxalic acid within spinach and tomatoes where these are processed within a blender and centrifuged at for 5 min. The supernatant was filtered via 0.45-mm filter paper and dispersed in perchloric acid with appropriate dilution, then 10 μL of the sample juice was added into the main electrochemical sensing cell; these measurements were validated against standard titration approach.

Enzymatic biosensors for the determination of oxalate has been reported [27–34]. In such cases, oxalate decarboxylase (EC 4.1.1.2) converts oxalate to formate and carbon dioxide, or oxalate oxidase (EC 1.2.3.4) converts oxalate stoichiometrically to hydrogen peroxide and carbon dioxide. For example, an enzymatic biosensor for determination of oxalate in different real food samples has been applied to spinach, sesame seed, tea leaves, strawberries and within human urine [35]. This sensor was constructed via the use of a chromium(III) hexacyanoferrate

**Table 1**
An overview of the electroanalytical sensors reported for the measurement of oxalate ($C_2O_4^{2-}$) and oxalic acid ($H_2C_2O_4$)

| Electrode material | Electrode modification | Electroanalytical Technique | Analyte | Dynamic Range | Limit of Detection | Real sample composition | Reference |
|---|---|---|---|---|---|---|---|
| CPE | OXO/HRP $TiO_2$/TB | Amp | $C_2O_4^{2-}$ | 0.1 - 2.0 mM | 0.09 mM | Spinach samples | [28] |
| Pt | Nylon membrane or a collagen membrane /OXO | Amp | $C_2O_4^{2-}$ | NR | 10 μM (collagen) 0.4 μM (Nylon) | NR | [27] |
| Clark-type $O_2$ electrode | Spinach (*spinacia oleracea*)/ OXO | Amp | $C_2O_4^{2-}$ | 10 - 100 μM | 10 μM | Urine | [29] |
| $CO_2$ sensor | Acrylamide gel – OXD | Amp | $C_2O_4^{2-}$ | 0 – 0.2 mM | 0.01 mM | Urine | [30] |
| GCE | OXO/SPAN/PB | Amp | $C_2O_4^{2-}$ | 0.08 – 0.45 mM | 0.08 mM | NR | [38] |
| GCE | OXO/PB | AMP | $C_2O_4^{2-}$ | 0.05 – 02.35 mM | NR | | [67] |
| Au | OXO/Au NPs/MWCNTs | CV | $C_2O_4^{2-}$ | 1 – 800 μM | 1 μM | Serum, urine and food stuffs | [31] |
| CPE | OXO/Sorghum leaves | Amp | $C_2O_4^{2-}$ | 20 – 200 μM | NR | Human urine and beer | [32] |
| Pt | OXO/ Sorghum leaves/c-MWCNTs/PANI | Amp | $C_2O_4^{2-}$ | 8.4 – 272 μM | 3 μM | Human urine | [68] |
| BPPG | NA | CV | $C_2O_4^{2-}$ | 2 – 30 μM; 0.5 – 3.5 mM | 0.7 μM | NR | [47] |
| Pt | $[Ru(bpy)_3]^{2+}$/ Nafion | CV | $C_2O_4^{2-}$ | 0.1 – 5 mM | 0.05 mM | NR | [41] |
| SPCE | $[Ru(bpy)_3]^2$ | CV | $C_2O_4^{2-}$ | 0.5 μM – 1 mM | NR | NR | [42] |
| Pt | OXO/mucin/carbopol | Amp | $C_2O_4^{2-}$ | 2 – 400 μM | 0.33 μM | Human urine | [69] |
| Graphite | OXO/CrHCF | Amp | $C_2O_4^{2-}$ | 2.5 – 400 μM | NR | Spinach, sesame seed, tea leaves, and strawberries and human urine | [35] |
| BDD | ATAB | Amp | $C_2O_4^{2-}$ | 0.8 – 100 μM | 32 nM | NR | [53] |
| CPE | Spongy osmium | FIA | $C_2O_4^{2-}$ | 0.05 – 350 μM | 10 nM | NR | [25] |
| AM | Graphite/carbon black/ castor oil/PLA | DPV | $C_2O_4^{2-}$ | 10 – 500 μM | 5.7 μM | Synthetic urine sample | [57] |
| Au | OXO/G@NPs/PPy/PANI/ CHIT | CV | $C_2O_4^{2-}$ | 1 – 400 μM | 1 μM | Human urine and plasma | [70] |
| Graphite | | DPV | $H_2C_2O_4$ | 0.1 – 0.7 mM | NR | Spiked tap water | [66] |
| Graphite | | AMP | $H_2C_2O_4$ | 0.5 – 3 mM | 0.05 mM | Spiked tap water | [71] |
| CPE | Silica - Nb NPs - HpCo | DPV | $H_2C_2O_4$ | 1456 - 4128 μM | 2.83 μM | NR | [64] |
| GCE | Palladium | LC-ED | $H_2C_2O_4$ | 0.2 – 1.2 μM | 0.15 μM | Human urine | [23] |
| GCE | Porous-$SiO_2$- Pt NPs | Amp | $H_2C_2O_4$ | 0 – 45 μM | 25 nM | Spinach and tomato | [26] |
| CPE | Pd Nanoparticles | CV | $H_2C_2O_4$ | 10 mM – 20 μM | 20 μM | NR | [19] |
| GCE | Pd/Polyvinylpyridine | CV | $H_2C_2O_4$ | 1 – 10000 μM | NA | NR | [24] |
| Graphite | OXO/CrHCF | Amp | $H_2C_2O_4$ | 2.5 – 100 μM | NR | Human urine | [37] |
| CPE | Cobalt Phthalocyanine | CV | $H_2C_2O_4$ | 0.1 – 2 μM | 0.12 μM | Human urine | [45] |
| CPE | Cobalt Phthalocyanine | CV | $H_2C_2O_4$ | 0.5 – 1000 μM | 50 nM | Human urine | [46] |
| BDD | gold | CV | $H_2C_2O_4$ | 10 – 100 μM | 135 nM | NR | [51] |
| BDD | FIA | CV | $H_2C_2O_4$ | 50 nM – 10 μM | 0.5 nM | NR | [50] |
| GCE | Rhodium phthalocyanin | Amp | $H_2C_2O_4$ | 10 - 300 μM | 1 μM | NR | [72] |
| CPE | Pd NPs - CNF | DPV | $H_2C_2O_{4ch}$ | 0.2 – 13 mM; 13 – 45 mM | 0.2 mM | Spinach | [65] |
| CPE | Carbon nitride | SWV | $H_2C_2O_4$ | 1 - 1000 μM | 0.75 μM | Human urine | [73] |
| GCE | Pt NPs - graphene | | $H_2C_2O_4$ | 0.1 – 15 mM; 15 – 50 mM | 10 μM | Spinach | [74] |
| GCE | PdPt NPs | AMP | $H_2C_2O_4$ | 10 μM – 11.8 mM | 1 μM | Spinach and Swiss chard | [75] |
| Tungsten carbide nanotubes | Pt NPs | AMP | $H_2C_2O_4$ | 0 – 125 nM | 12 nM | Tomato juice | [56] |
| GCE | MWCNTs | DPV | $H_2C_2O_4$ | 50 μM – 15 mM | 12 μM | Spinach | [76] |
| GCE | Pd NPs/PAMAM-MWCNTs | CV | $H_2C_2O_4$ | 0.03 – 5 mM | 0.02 mM | Spinach | [54] |
| GCE | Pt-Pd NPs/Chit/N-Graphene | DPV | $H_2C_2O_4$ | 1.5 – 500 μM | 0.84 μM | Vitamin C injection | [63] |
| GCE | Silver nanorods-graphene | CV | $H_2C_2O_4$ | 3 – 30 mM | 0.04 mM | Tap water | [55] |
| SPCE | Pt/CB-Ni-rGO | AMP | $H_2C_2O_4$ | 20 μM – 60 mM | 2.35 μM | Artificial urine | [77] |
| GCE | MIP-$W_2C$ | DPV | $H_2C_2O_4$ | 0.1 nM – 100 μM | 0.04 nM | Human urine | [61] |

**Key:** CPE: carbon paste electrode; OXO: oxalate oxidase; HRP: horseradish peroxidase; $TiO_2$: titanium oxide; TB: toluidine blue; OXD: oxalate decarboxylase; SPAN: self-doped polyaniline; PB: Prussian blue; Au NPs; gold nanoparticles; MWCNTs: multi-walled carbon nanotubes; CrHCF: chromium(III) hexacyanoferrate(II) film; $[Ru(bpy)_3]^{2+}$: tris(2,2'-bipyridine)ruthenium(II); FIA: flow injection analysis; BDD: boron-doped diamond; LC-ED: liquid chromatography – electrochemical detection; CV: Cyclic voltammetry; Amperometry: AMP; ATAB: Allyltriethylammonium bromide; AM: additive manufacturing; DPV: differential pulse voltammetry; PLA: poly(lactic acid); FIA: flow through injection analysis; PSiO: porous silica; NPs: nanoparticles; N-Graphene: nitrogen-doped graphene; Chit: chitosan; MIP: molecularly imprinted polymer; c-MWNCTs: carboxylated multiwalled carbon nanotubes; PANI: polyaniline; SPCE: screen-printed carbon electrodes; RGO: reduced graphene oxide; CB: carbon black; SWV: square-wave voltammetry; G@NP: graphene oxide nanoparticles; PPy: polypyrrole; HpCo: cobalt hematoporphyrin; CNF: carbon nanofibers; PAMAM: polyamidoamine dendrimer; NR: not reported.

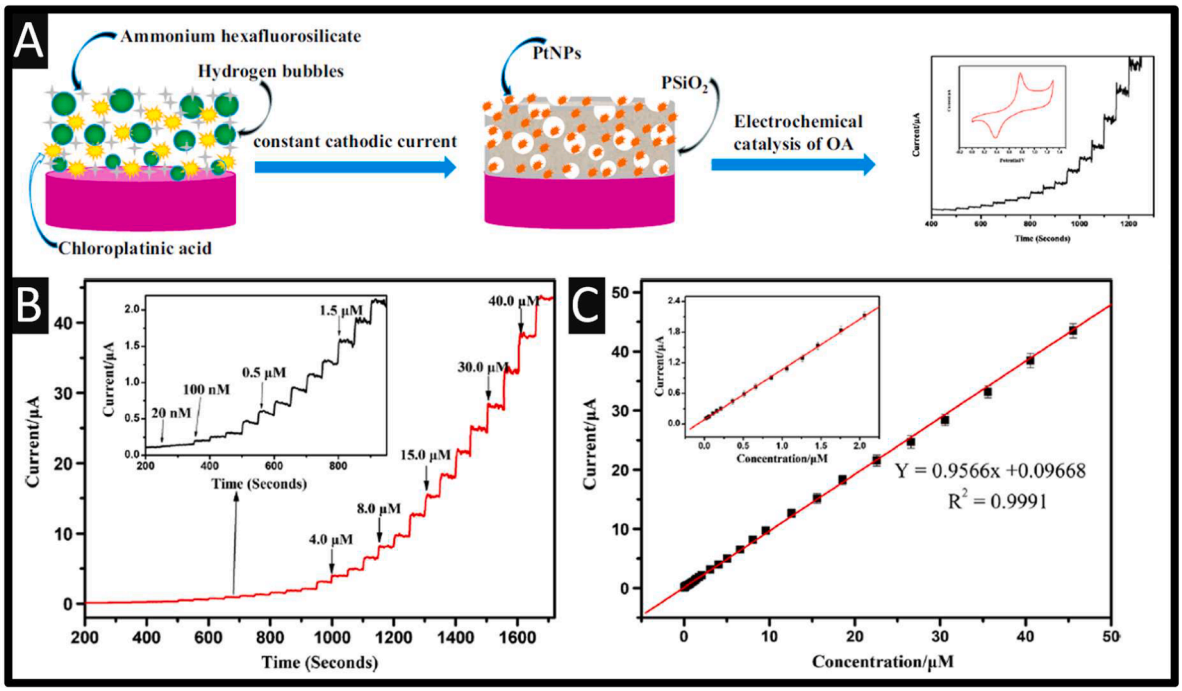


**Fig. 1.** **A**: An overview of the construction of the sensor; **B**: Amperometric curves obtained using the porous$SiO_2$-Pt NPs sensor from the additions of oxalic acid; **C**: Corresponding calibration curve. Reproduced with permission from reference [26]. Copyright 2020 Springer.

(II) film, which was immobilized upon a graphite electrode using a bovine serum albumin and glutaraldehyde cross-linking procedure. The electrocatalytic response was attributed to:

$$H_2CO_4 + O_{ox}(FAD) \rightarrow 2CO_2 + O_{ox}(FADH_2) \quad (6)$$

$$O_{ox}(FADH_2) + O_2 \rightarrow O_{ox}(FAD) + H_2O_2 \quad (7)$$

Noting that chromium (III) hexacyanoferrate(II) film has been used for the electrocatalytic determination of hydrogen peroxide [36,37], which can be considered as: $H_2O_2 + 2[Cr(CN)]_6^{4-} \rightarrow 2OH^- + Cr(CN)]_6^{3-}$ this, plus operating with Eqs. (6) and (7), gives rise to the overall observed electrocatalytic response. This chromium (III) hexacyanoferrate(II) film also allows a lower overvoltage of hydrogen peroxide thus voiding the possible oxidation of interferences. The authors reported a linear range from 2.5 to 400 μM while noting that time of analyses with the biosensor (sample and four internal additions of standard solutions) is approximately 8 minutes which is significantly shorter than the time necessary for oxalate determination with spectrophotometric enzymatic method, which can take more than one hour [35]. The use of a Prussian Blue film covered self-doped polyaniline layer with oxalate oxidase has been shown to act as amperometric sensor for the $H_2O_2$ formed by the enzymatic reaction [38]. This sensor reports a linear response from 0.08 to 0.45 mM where the films lead to a stable and selective system that minimizes the interference by ascorbic and uric acids.

Other work has explored the case of two amperometric biosensors formed by immobilization of oxalate oxidase on collagen and Nylon membranes. The experimental set-up uitlised a platnium anode, which electrochemically oxidised the hydrogen peroxide that is produced via the presense of oxalate oxidase, and undergoes a two-electron reaction. The authors found that the Nylon based sensors (0.4 μM) has a much lower detection limit over that of the collagen (10 μM), where Nylon has advantages include a higher degree of flexibility, mechanical durability, wider pH range for utilization, greater specific activity and lower limit of detection, suggesting that Nylon is utilized in future biosensors for the sensing of oxalate. Other work has developed a enzymatic biosensor utilizing two enzymes, oxalate oxidase and horseradish peroxide which were incorporated into a carbon paste electrode. The paste electrode was modified with silica gel coated with titanium oxide containing toluidine blue [28]. This sensor was able to measure oxalate over the range of 0.1 – 2.0 mM with a LoD reported to be 0.09 mM. Critically, the authors measure the amount of oxalate within spinach samples and compared their method with the Association of Official Agricultural Chemists (AOAC) 974.24, which involves spectrophotometry. The authors found their result showed a difference from 7 to 13%, where the biosensor measures oxalate at higher values since the AOAC has many precipitation steps, which can cause a loss of some oxalate, decreasing the results [28]. The biosensor has many advantages which included: low cost, rapid, 1 min for the biosensor and 5 minutes for the AOAC method, and it generates no chemical residues.

One interesting approach has utilized electrogenerated chemiluminescence for the measurement of oxalate [39–43], where electrochemically generated intermediators that undergo high-energy electron-transfer reactions to form light-emitting excited states. For example, Egashira and co-workers [41] have reported on a electrochemiluminescence sensor based upon the use of a tris(2,2′-bipyridine) ruthenium(II) ($[Ru(bpy)_3]^{2+}$) Nafion-modified platinum gauze electrode for the sensing of oxalate. The suggested electrochemical mechanism as illustrated below:

$$[Ru(bppy)_3]^{2+} \rightarrow [Ru(bppy)_3]^{3+} + e^- \quad (8)$$

$$[Ru(bppy)_3]^{3+} + (COO)_2^{2-} \rightarrow [Ru(bppy)_3]^{2+} + (COO)_2^{\bullet -} \quad (9)$$

$$(COO)_2^{\bullet -} \rightarrow (CO)_2^{\bullet -} + CO_2 \quad (10)$$

$$[Ru(bppy)_3]^{3+} + (CO)_2^{\bullet -} \rightarrow [Ru(bppy)_3]^{2+*} + CO_2 \quad (11)$$

$$[Ru(bppy)_3]^{2+*} \rightarrow [Ru(bppy)_3]^{2+} + hv \quad (12)$$

The authors found that their sensor was linear over the range of 0.1 to 5 mM with an LoD was 0.05 mM, however found their sensor responded to other carboxylic acids and amino acids but being weaker than that to oxalate. It was noted that the response to 0.5 mM oxalate was reproducible within 3% on 10 repeated runs and the sensor response was unchanged over 10 days [41].

Others have utilized disposable screen-printed carbon electrode for simultaneous electrochemiluminescence and amperometric detection in sequential injection analysis which can detect oxalate over a four-order range [42] as well as the use of a fibre optic electrochemiluminescence for the measurement of oxalate within spinach [43] and urine [44]. The use of cobalt phthalocyanine (CoPC) as an electrocatalyst has been employed for the measurement of oxalic acid [45,46]. This sensor was fabricated by the mixing of CoPc with the graphite and Nujol oil which was shown to provide a linear range of 0.5 – 1000 μM, with a LoD reported to be 50 nM. This sensor was applied to measured oxalate within urine samples where it was collected from a healthy volunteer, filtered by passing through a -15-μm glass filter and diluted. This approach has been extended to co-electroosmotic capillary electrophoresis with amperometric detection which was applied to the sensing of oxalic acid within spiked urine samples [46].

Šljukić and co-workers [47] explored the electrochemical oxidation of oxalate but explored the response at different carbon electrodes, namely: basal and edge plane pyrolytic graphite (BPPG and EPPG) and glassy carbon electrodes (GC) – please see Fig. 2A for the electrochemical responses. This electrode are utilized to gauge the reversibility of the electrochemical response, where pyrolytic graphite is an electrode material which contains both basal plane and edge plane surfaces, with the graphite monocrystal size and basal/edge ratio depending on the quality of the used pyrolytic graphite. Due to the nature of the chemical bonding in graphite, the two planes, edge and basal exhibit different electrochemical properties where for instance the electron-transfer rate constants at edge plane graphite have been found to be over ~$10^3$ times faster than for basal plane graphite [48]. As can be observed, a chemically irreversible peak corresponding to the oxidation of oxalate where the oxidation peak of oxalate oxidation at GC electrode appeared at high potential of +1.44 V (vs. SCE) whereas at BPPG and EPPG electrodes appeared at lower potentials, +1.13 and +1.20 V (vs. SCE) respectively, and with peak currents higher than one obtained at GC electrode. This response is due to the fact that carbon electrode reactivity is dependent on the analyte being measured, influenced by surface cleanliness, surface microstructure, hydrophobicity/hydrophilicity, electronic structure, *i.e.,* density of states and surface carbon oxides [47]. The authors report that the electrochemical mechanism is reported as:

$$C_2O_4^{2-}\text{-}2e^- \rightarrow 2CO_2 \quad (13)$$

The diffusion coefficient was also found to be 1.03 × $10^{-5}$ $cm^2$ $s^{-1}$. The authors chose to explore the BPPG electrode towards the sensing of oxalate and as shown within Fig. 2B and C, the cyclic voltammetric response is show for the following ranges: 2 - 30 μM and 0.5 – 3.5 mM with a LoD reported to be 0.7 μM. The LoD is comparable or lower than those obtained by enzymatic biosensors without the use of expensive chemicals and complicated procedures [47].

One intriguing approach is the use of an applied magnetic field towards the measurement of oxalate [49]. Through the use of two flat foil plate electrodes as both the working and counter electrodes and a Ag/AgCl electrode as the reference electrode, using a large magneto-current the electrochemical oxidation of oxalate increased by 30% where the large MC is ascribed to spin-dependent oxidation of oxalate; see Fig. 3A for the mechanism. The proposed mechanism is show below [49]:

$$C_2O_4^{2-}\text{-}e \rightarrow C_2O_4^{-\bullet} \quad (14)$$

$$C_2O_4^{-\bullet} \rightarrow CO_2 + CO^{-\cdot}{}_2 \quad (15)$$

$$^1[CO^{-\cdot}{}_2 \uparrow + CO^{-\cdot}{}_2 \downarrow] \rightarrow C_2O_4^{2-} \quad (16\text{-}1)$$

$$^3[CO^{-\cdot}{}_2 \uparrow + CO^{-\cdot}{}_2 \uparrow] \neq C_2O_4^{2-} \quad (16\text{-}2)$$

$$CO^{-\cdot}{}_2\text{-}e \rightarrow CO_2 \quad (17)$$

where the oxidation of oxalate undergoes electron transfer, Eqs. (14) and (17), the dissociation into radical anions (Eq. 15) and the recombination (Eq. 16) where the steps are consecutive.

The large magneto-current is attributed to spin-dependant oxidation of oxalate where both singlet and triplet radial pairs are generated where the magnetic fields accelerate the spin evolution of a signal radical pair into its triplet state (see Fig. 3A) [49]. As shown within Fig. 3B, the amplitude of magneto-current increases as the oxalate concentration is increased while in Fig. 3C, the maximal amplitude of magneto-current is linear related to the concentration of oxalate [49].

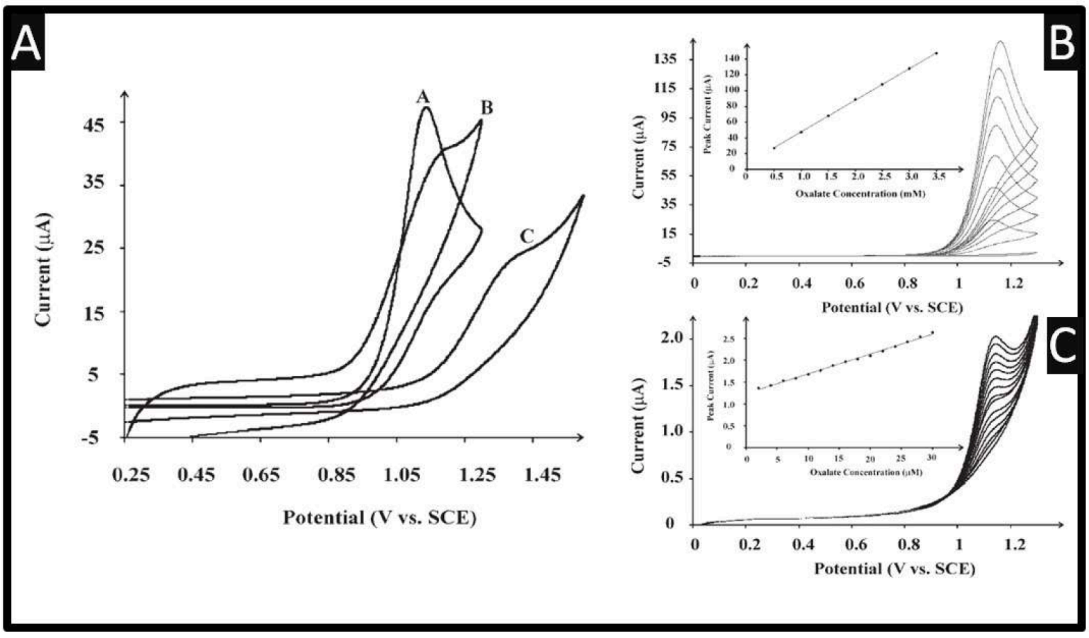


**Fig. 2.** **A**: Cyclic voltammograms of BPPG (A), EPPG (B), and GC (C) electrode recorded in 1 mM oxalate solution / 0.1 M $K_2SO_4$. Scan rate: 50 mV $s^{-1}$. **B**: Cyclic voltammograms of BPPG electrode in 0.1 M $K_2SO_4$ with increasing oxalate concentration from 0 to 3.5 mM at scan rate of 50 mV $s^{-1}$ and **C:** linear sweep voltammograms of BPPG electrode in 0.1 M $K_2SO_4$ with increasing oxalate concentration from 0 to 30 μM; Scan rate: 50 mV $s^{-1}$. Reproduced with permission from ref [47]. Copyright 2007 Wiley.

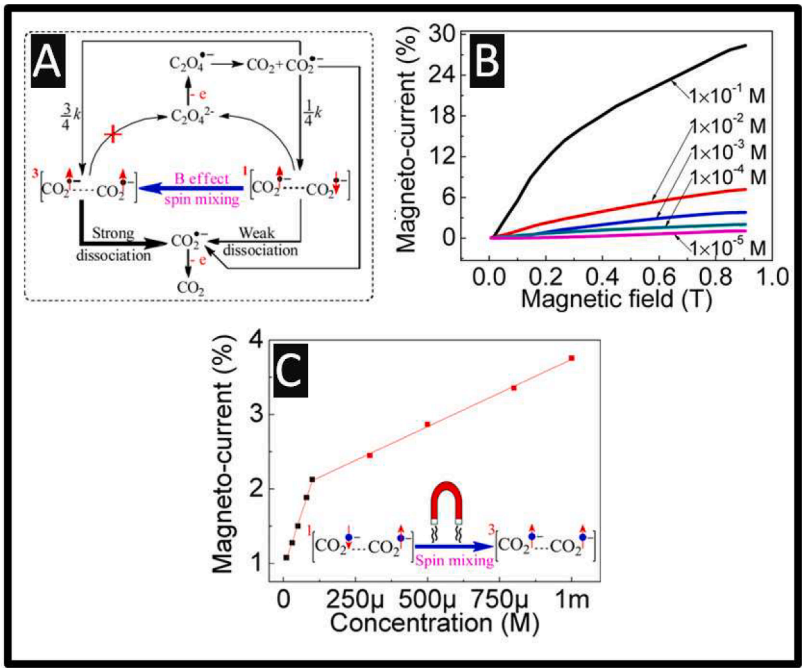


**Fig. 3. A:** Proposed mechanism is shown for electrochemical oxidation process of oxalate under magneto-current; **B:** Magneto-current is shown for different concentrations of sodium oxalate dissolved in water at +1.5 V applied electrode potential**; C:** Amplitude of magneto-current is linearly related to the concentration of oxalate over the region 10 μM to 100 μM and 100 μM to 1 mM in the magnetic field of 0.9 T. Reproduced from reference [49]. Copyright 2018 American Chemical Society.

This work has merits in improving the electroanalytical response towards oxalate, but it needs to be applied into real samples.

One of the most sensitive sensors are based upon a boron-doped diamond electrodes (BDD) towards oxalate [50,51]. BDD doping with greater than $10^{20}$ atoms $cm^{-3}$ makes BDD metallic and it is widely used for electrochemical applications due to its low background current, broad potential window, and resistance to fouling; please see reference [52] for an overview. The authors considered the use of gold nanoparticle dispersed-BDD (Au-np-BDD) fabricated by physical deposition (laser ablation method) and gold-implanted BDD (Au-i-BDD) for the sensing of oxalic acid [51]. Fig. 4A shows the position of the gold nanoparticles, ~ 4.6 nm in diameter and also are presented the cyclic voltammogram responses (Fig. 4B) where the as-deposited BDD (AD BDD), and Au-i-BDD gave a well-defined peak was observed at the potential of +1.3V (vs Ag/AgCl) at Au-np-BDD which is relatively similar to the oxidation potential at Au-i-BDD (+1.3 V) and at as-deposited (AD) BDD (+1.2 V) than at gold metal bulk (+0.8 V) electrode. Clearly the way the electrodes were fabricated gives rise to the beneficial electrochemical response towards oxalate. The authors explored the use of the Au-np-BDD electrodes for the sensing of oxalate which gave a linear range from 10 to 100 μM where the LoD was reported to be 135nM which was ~16 times lower than that of the gold metal. Furthermore, work has utilized hydrogen-terminated BDD using cyclic voltammetry and flow injection analysis with amperometric detection [50]. As shown within Fig. 4C, cyclic voltammetric profiles are observed +1.32 V (vs Ag/AgCl where a linear response was observed for over the range 10-100 mM (Fig. 3B). Also shown in Fig. 4C is the repetitive cyclic voltammogram where no significant deviations were observed up to 50$^{th}$ cycles. Of further note, oxygen-terminated BDD showed no response for oxalic acid oxidation indicating that surface termination contributed highly to the control of the oxidation reaction [50]. This sensor was shown via flow injection analysis that a linear range of 50 nM to 10 μM is possible with an LoD reported to be 0.5 nM.

A hydrogen terminated boron-doped diamond (BDD) electrodes have been modified with Allyltriethylammonium bromide (ATAB) which was covalently attached to the which was explored to the measurement of oxalate [53]. Using flow injection analysis, the authors showed that the current was up to two times larger at ATAB-modified BDD than at an unmodified BDD electrode, which may be based on the electrostatic interaction between the oxalate anion and the electrode surface. Furthermore the stability of the electrochemical detection of oxalate was improved at the ATAB-BDD electrode compared to the unmodified (bare) electrode [53]. This sensor was shown to provide a low detection range of a LoD reported to be 32 nM with a linear range of 0.8 - 100 μM.

As shown within Fig. 5A, a palladium nanoparticles - polyamidoamine dendrimer-grafted multi-walled carbon nanotubes hybrid was fabricated [54]. In their approach, amino functionalized multi-walled carbon nanotubes were synthesized by a click reaction between propargyl-functionalized MWCNTs and 3-azidopropylamine [54]. Next, polyamidoamine dendrimers are synthesized where the amino-multi-walled carbon nanotubes are functionalized into ester-multi-walled carbon nanotubes which then ethylenediamine is added into form the polyamidoamine dendrimer-grafted multi-walled carbon nanotubes. Last, palladium nanoparticles are added via the use of the palladium salt using a reducing reagent which results in.an average diameter of 1.8 – 2.8 nm. This composite is shown that oxalic acid can be measured over the range of 0.03 – 5 mM with a LoD of 0.02 mM; this was shown to sense oxalic acid within spinach with the authors noting that surface fouling does not occur where they can use their sensor more than 130 analysis [54].

An interesting approach has utilized the electrochemical synthesis of graphene functionalized with silver nanorods using 3D surfactant 4-sulphocalix [4] arene and silver nitrate [55]. The authors used electrochemical exfoliation of graphite, using two graphite rods within 4-sulphocalix [4]arene with silver nitrate where a constant voltage of 10 V was applied for 6 hrs. This approach produced silver nanorods with 700 nm and 60 nm dimensions. This approach allowed the detection of oxyalic acid from 3 to 30 mM with a LoD of 0.04 mM. The interference of metal ions, $Mg^{2+}$, $Ca^{2+}$, $Zn^{2+}$, $Ni^{2+}$ and $Co^{2+}$ and biomolecules such as ascorbic acid and uric acid were tested where it is reported that the sensor response towards oxalic acid change only +/- 5% but the $Co^{2+}$ decreased the current forming a complex with oxalate [55]. Last, the

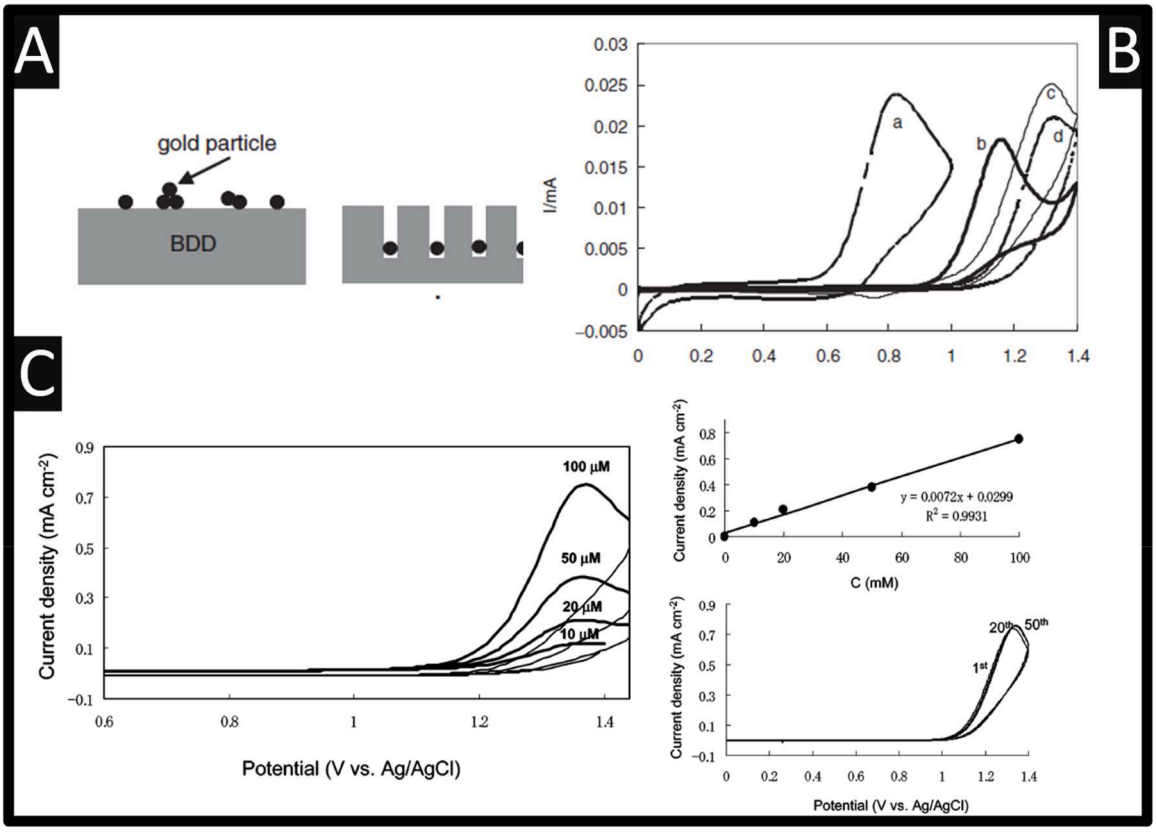


**Fig. 4.** **A**: Position image of gold particles at a gold-nanoparticle dispersed BDD (left image) and a gold-implanted BDD (right image); depth ~ 200 nm). **B**: Cyclic voltammograms of 100 mM oxlic acid in 0.1M phosphate buffer solution pH 7 at gold (a); as-deposited BDD (b); gold-nanoparticle-dispersed BDD (c) and gold implanted DD (d); scan rate: 100 $mVs^{-1}$ scan rate. Reproduced from reference [51] Copyright 2005 The Chemical Society of Japan. **C**: Cyclic voltammograms of oxalic acid in various concentrations in 0.1 M phosphate buffer solution, pH 2.1, at as-deposited diamond electrode. Scan rate was 100 $mVs^{-1}$. The bold and thin line show forward and reverse scans, respectively. Insets show (a) linear dependence of the current density on oxalic acid concentration and (b) repetitive cyclic voltammograms of 100 µM oxalic acid solution with a quiet time of 1 min between cycling. Reproduced from reference [50]. Copyright 2006 American Chemical Society.

sensor was shown to be successful in detecting oxalic acid within spiked tap wasters with recoveries between 100 to 102%.

An innovative approach has fabricated tungsten carbide nanotubes supporting platinum nanoparticles [56]. As shown within Fig. 5C, the tungsten carbide nanotubes are fabricated through taking ammonium meta-tungstate and glucose which are placed into a Teflon-lined steel autoclave where a porous anodized alumina membrane is also place on the solution, where the reaction mixture was autoclaved for 25 hrs at 180 degrees. This membrane is removed and carbonized at 900 degrees within a tube furnace for 4 hrs. The TEM and SEM of the fabricated tungsten carbide nanotubes can be seen within Fig. 5C. The tungsten carbide nanotubes are then plating with platinum nanoparticles by adding in a acid salt which are reduced by flowing hydrogen gas at 550 degrees [56]. This sensor exhibited a concentration ranges from 0 to 125 nM and a LoD of 12 nM which it is attributed to the unique geometry of the high surface area and a higher total pore volume allowing more amounts of platinum nanoparticles (~3 nm diameter) to be available to electrochemical oxidize the oxalic acid; the sensor was demonstrated to be successful for the detection of oxalic acid in tomato fruit sample [56].

The use of additive manufacturing has been reported for the electroanalytical measurement of oxalate [57]. The use of additive manufacturing within electrochemical research has gained recognition due to its plethora of benefits [58–60] which include: rapid prototyping capabilities, in-situ production, reduced waste production and low cost of entry. The use of additive manufacturing has also the advantages in efficiency when compared to traditional prototyping methods, which stands out due to the ability to produce different types and designs of devices on the same printer without retooling, giving substantial production potential and adaptability [60]. In their work, Arantes et al., [57], they reported upon the development of conductive filament through a composite of nano carbon black and graphite in recycled PLA, with the bio-based plasticizer, castor oil, to increase the low-temperature flexibility of the filament.

As shown within Fig. 6, an overview is presented which shows how 65 wt% rPLA, 10 wt% castor oil, 15 wt% nano carbon black, and 10 wt% graphite powder are extruded which makes the filament of the chosen diameter, which is then applied to a spool which is connected to a fused filament fabrication printer which allows the working electrode to be realized. This bespoke approach is highly novel which results in an electrode surface that exhibits electrochemical performance over that of a commercially available filament, due to the former approach using high amounts of conductive material, while also being highly printable and yet being low cost. This sensor was shown to report a dynamic range from 10 to 500 µM with a LoD of 5.7 µM; and used for the successful in the determination oxalate with a spiked synthetic urine sample. This work highlights how using mixed carbon material composites can create conductive filaments with beneficial electrochemical properties with lower material cost whilst using recycled polymer and bio-based plasticizers to improve the sustainability of the filament process [57].

Another useful approach is the use of molecular imprinted polymers (MIP) coupled with $W_2C$ nanoparticles [61], where MIP are an interesting appeal to researchers since they represent synthetic recognition elements that can be matched towards a biomarker target [62]. A facile but yet non-toxic approach was used by Hussain and co-workers [61]

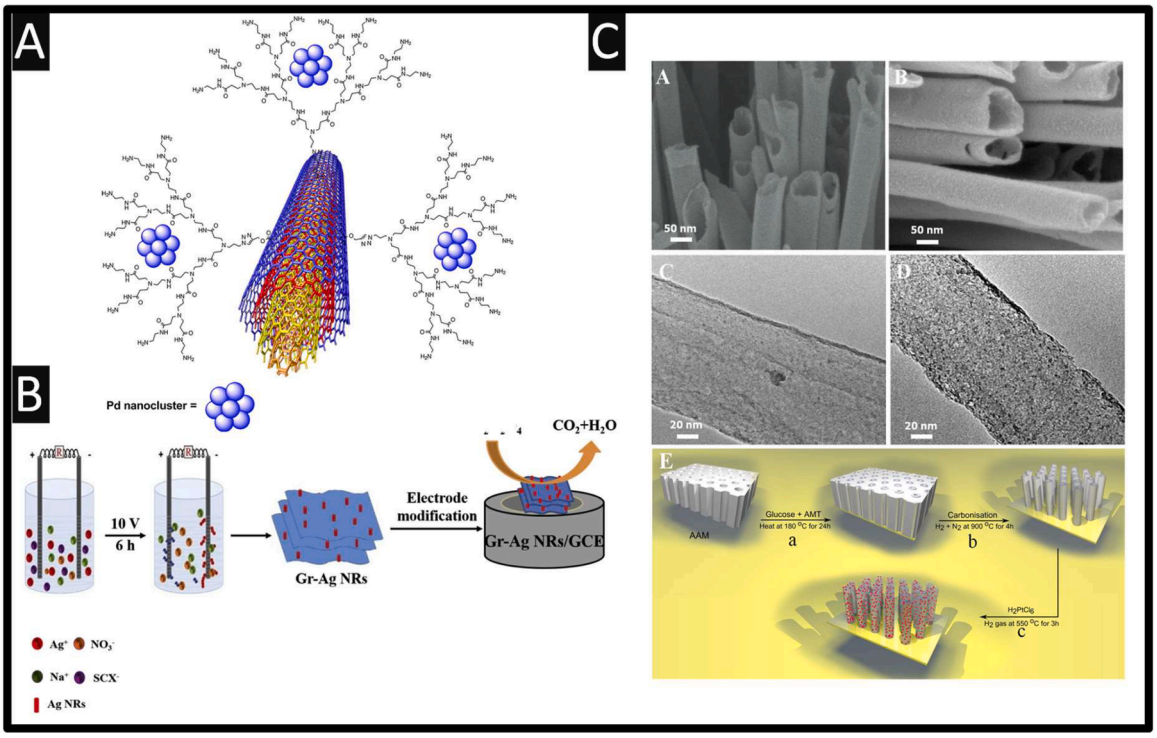


**Fig. 5.** **A**: An overview of the palladium nanoparticles - polyamidoamine dendrimer-grafted multi-walled carbon nanotubes hybrid. Reproduced from reference [54]. Copyright 2012 Elsevier. **B:** A summary of how to obtain graphene functionalized with silver nanorods using 3D surfactant 4-sulphocalix [4]arene and silver nitrate from an aqueous solution. Reproduced from reference [55]. Copyright 2019 Elsevier. **C:** High-resolution SEM and TEM images of before (a and c) and after (b and d) loading of platinum nanoparticles into the surface walls of tungsten carbide nanotubes. A uniform dispersion of platinum nanoparticles (black dots) is clearly visible on the surface of tungsten carbide nanotubes (d). The corresponding schematic representation of the platinum nanoparticles loaded on the surface of tungsten carbide nanotubes (e). Reproduced from reference [56]. Copyright 2014 American Chemical Society.

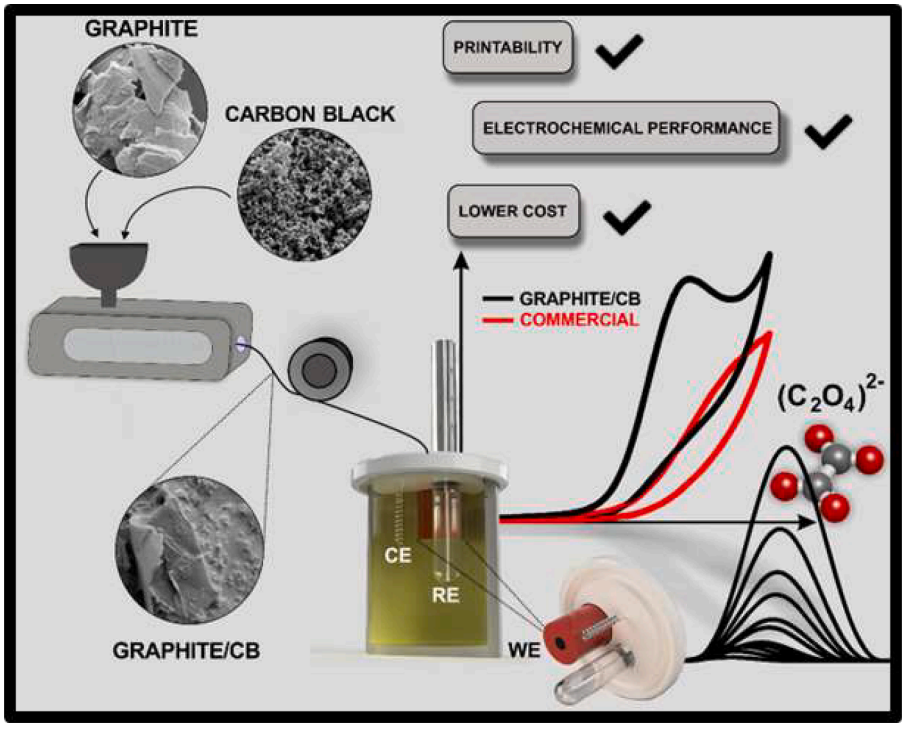


**Fig. 6.** An overview of how the bespoke additive manufacturing filament where nano carbon black and graphite are incorporated within recycled PLA and castor oil which it is extruded, which results in a highly printability filament which has a lower cost and enhanced electrochemical performance compared to commercially available filament. Reproduced from reference [57]. Copyright 2023 American Chemical Society.

where they obtained $W_2C$ powder from a commercial source where it was dispersed into ethanol and continuously stirred for 3 h at room temperature; see Fig. 7(A-D). Next liquid ammonia was added to the solution which it was kept in an oven at 85°C for 5 h under vigorous stirring. The resulted sediment was cleaned using water, centrifuged, and kept in an oven overnight at 60°C for drying. The powder was then placed under a gas mixture of hydrogen, and methane gas in a tubular furnace at 850°C for 3 h as the annealing process producing $W_2C$ nanoparticles which can be seen within Fig. 7 (E-J) reported that the diameters were 21.4 nm.

The MIP was formed via self-polymerization where a $W_2C$ nanoparticle covered GCE is exposed to a solution comprising oxalate and dopamine within a pH 8.5 which was left for 3 h. the oxalate were extracted from the polymer matrix in an acetic acid and acetonitrile solution with slight stirring to achieve an MIP-$W_2C$/GCE where the use of dopamine forms polydopamine which acts as the MIP oxalate sensor. A similar preparation and washing steps were followed for the non-imprinted polymer (NIP-$W_2C$/GCE) sensor except the addition of oxalate. It is well known that the MIP film thickness affects its recognition behaviour. The observed thickness of the MIP, $d_{thickness}$ can be deduced via:

$$d_{thickness} = MQ/FA\rho \tag{18}$$

where $\rho$ is the density of the polymer, $M$ is the molecular weight of the monomer, $Q$ is the charge represents transferred charge which was acquired by the related cyclic voltammetric profile integration, $F$ is the Faraday constant and $A$ is the electrode area. The authors reported that their MIP film layer corresponds to 2.9 nm, where the use of 3 h provides the optimal thickness [61]. Through the use of differential pulse voltammetry, a linear response towards oxalate is possible over the range of 0.1 nM to 100 μM with a LoD reported to be 0.04 nM; see Fig. 7 where also shown is the selectivity towards uric acid, creatinine, urea and ascorbic area where they are added 60 times higher than that of oxalate which show negligible response to the interferents. Last, this sensor was shown to be useful for the measurement of oxalate within spiked human urine which shows recovers in the range 98.03 – 100.24 %; this sensor has promising to be used as a regular response to the measurement of oxalate within biological samples.

One of the few reports that have been reported towards the oxalate in the presence of other analytes, is exemplified within Fig. 8. In their approach, the authors took a GCE which was modified with nitrogen-doped-graphene which it is dissolved within 1% chitosan which was dried under an infrared lamp. Next, the Pt-Pd nanoparticles are formed via electrochemical deposition through applying cyclic voltammetry where the potential is held at -0.4 V for 90 seconds.

The author utilised their composite electrode towards the simultaneous determination of ascorbic acid, sulfite and oxalic acid where in the case of oxalic acid, a LoD was reported to 0.84 μM with a linear range from 1.5 to 500 μM. As can be observed from Fig. 8A, the voltammetric peaks are well-resolved after which the authors optimised the concentration ratio of the platinum and palladium salt precursors as well as pH which the sensing was performed. The authors used their sensor to measure ascorbic acid within a vitamin C injection as well as the monitoring of sulphite, which it is used as a stabilizer and oxalic acid which it is an impurity [63], reported recoveries in the range of 92.7 – 105% with a RSD less than 7.4%. Other work has reported the simultaneous sensing of oxalic acid and 4-chlorophenol using an expanded graphite-epoxy composite electrode, where the electrochemical oxidation of oxalic acid and 4-chlorophenol are observed at +1.1 V and +0.8V (*vs.* SCE) which was sufficient for the sensing of oxalic acid over the

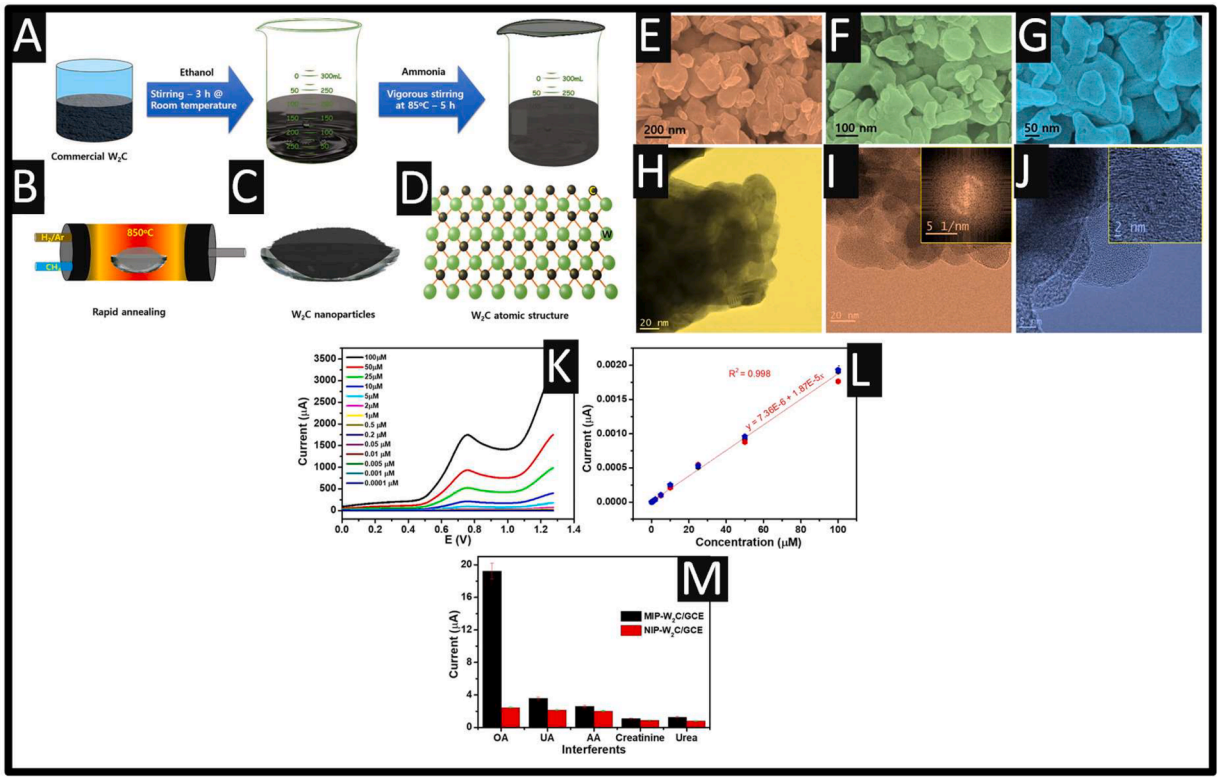


**Fig. 7.** An overview of how the $W_2C$ nanoparticles are produced, where the formation procedure is: $W_2C$: (A) chemically modification, (B) 850°C annealing in the tubular furnace, (C) the resultant powder, and (D) $W_2C$ atomic arrangements. Also show are the (E, F and G) field emission scanning electron microscopy and (H, I, J) transmission electron microscopy micrographs for chemically modified $W_2C$ nanoparticles. Differential pulse voltammetry of oxalate in the concentration range of 0.0001–100 μM (K) and (L) Calibration plot obtained corresponding to oxalate concentrations (0.0001–100 μM, mean of triplicated results) with error bars from the triplicated results. (M) Selectivity of oxalate (1 μM) with the existence of other interfering compounds (each 60 μM) using MIP-$W_2C$ and NIP-$W_2C$ sensors with error bars from the triplicated results. Electrolyte: 0.1 M PBS (pH 7.0) and scan rate: 0.1 V $s^{-1}$. Reproduced from reference [61]. Copyright 2020 Elsevier

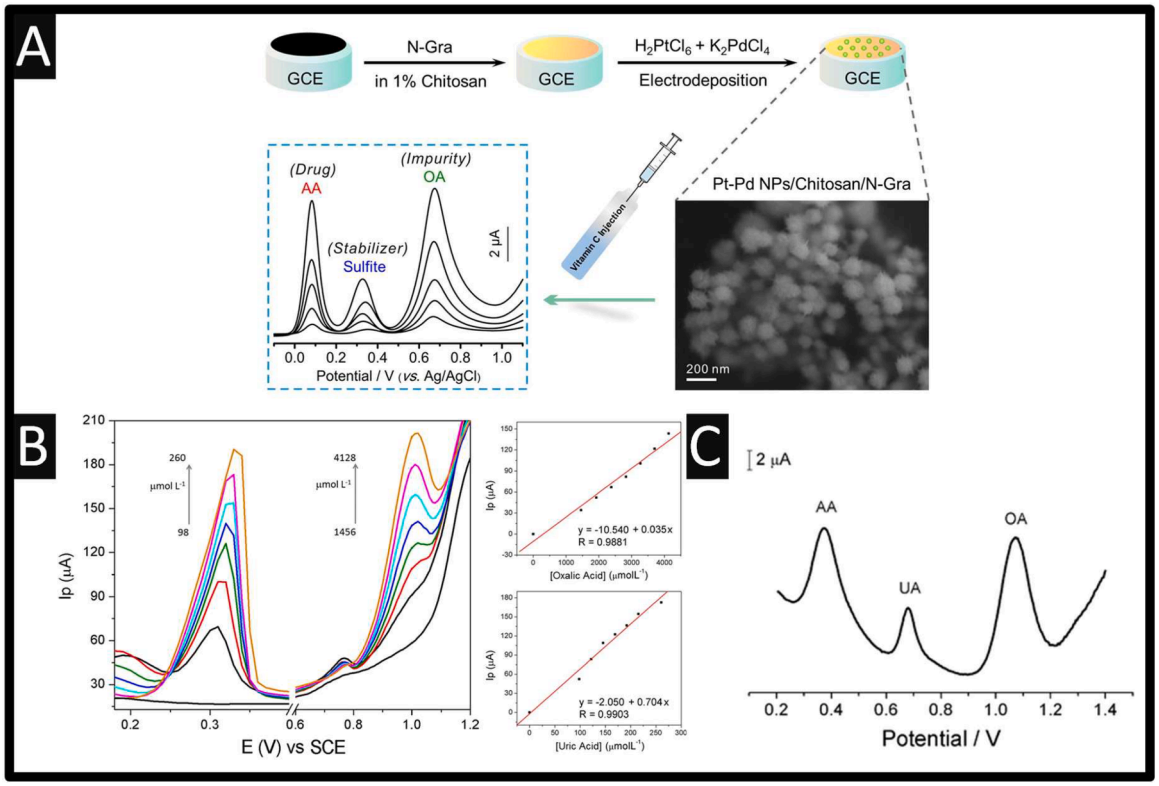


**Fig. 8.** **A:** An overview of the simultaneous detection of ascorbic acid, sulphite and oxalic acid which also shows how the fabrication of the electrochemical sensing platform is produced. Reproduced from reference [63]. Copyright 2021 Elsevier. **B:** Simultaneous analysis performed using differential pulse voltammetry for oxalic and uric acids using the SBA/Nb/HpCo–CPE. Linear correlation between oxalic acid and uric acid concentrations and peak current intensities. Reproduced from reference [64]. Copyright 2021 Springer Link. **C:** Differential pulse voltammetry recorded at a palladium nanoparticles modified carbon nanofibre containing 10 mM ascorbic acid, 0.5 mM uric acid and 10 mM oxalic acid. Reproduced from figure [65]. Copyright 2010 The Royal Socieyt of Chemistry.

range 0.1 to 0.7 mM which allowed the authors to measure within spiked tap water [66]. Souza and co-workers [64] have reported the simultaneous sensing of oxalic and uric acids which reports a linear range for oxalic acid from 1456 to 4128 μM with a LoD reported 2.83 μM; see Fig. 8B This sensor was comprised of SBA-15 type silica (500 nm diameter) which was surface modified with niobium oxide which cobalt hematoporphyrin which results in a high porosity surface. That said, in sensing of oxalic acid in the presence of uric acid, the linear range is rather high compared to other approaches (see Table 1) and the sensor needs to be evaluated within real samples. Last, the sensing of the simultaneous determination of oxalic, uric and ascorbic acids has been reported [65]. As shown within Fig. 8C, the differential pulse voltammetry is shown where each peak are observed at + 0.37, + 0.68 and + 1.07 V, corresponding to the ascorbic acid, uric acid and oxalic acid which are all resolved from each other. This sensor was comprised of palladium nanoparticles upon carbon nanofibers where the latter were fabricated by carbonizing electrospun polyacrylonitrile – palladium salt which resulted in carbon nanofibers with diameter from 300 to 500 nm with palladium nanoparticle embedded. This sensor was able to measure oxalic acid in the presence of ascorbic and uric acids over the range of 0.2 – 13 mM and 13 – 45 mM with a LoD reported to be 0.2 mM. which was successfully applied to the sensing oxalic acid within spinach.

**Table 2**
A summary of the analytical approaches for the measurement of oxalate.

| Approach | Analyte | Dynamic Range | Limit of Detection | Real sample composition | Reference |
|---|---|---|---|---|---|
| Fluorescence | $C_2O_4^{2-}$ | 1 – 5 μM | 0.079 μM | NR | [12] |
| Liquid Chromatography–Tandem Mass Spectrometry | $C_2O_4^{2-}$ | NR | 3 μM | Human urine | [78] |
| Luminescence | $C_2O_4^{2-}$ | 10 nM – 400 μM | 10 nM | NR | [14] |
| Chemosensor | $C_2O_4^{2-}$ | 0.8 – 113 μM | 0.54 μM | Human urine | [79] |
| Colorimetric | $C_2O_4^{2-}$ | 7.8 - 2500 μM | 0.91 μM | Artificial urine | [80] |
| Fluorescence | $C_2O_4^{2-}$ | 1 – 50 μM | 0.69 μM | Human urine | [81] |
| Microchip electrophoresis | $C_2O_4^{2-}$ | 500 nM – 300 μM | 19 nM | Aerosol sample | [82] |
| Electrochemical | $C_2O_4^{2-}$ | 0.8 – 100 μM | 32 nM | NR | [53] |
| Electrochemical | $C_2O_4^{2-}$ | 1 – 800 μM | 1 μM | Serum, urine and food stuffs | [31] |
| Electrochemical | $H_2C_2O_4$ | 0 – 45 μM | 25 nM | Spinach and tomato | [26] |
| Electrochemical | $H_2C_2O_4$ | 0 – 125 nM | 12 nM | Tomato juice | [56] |

## 3. Conclusion and outlook

We have overviewed the electroanalytical approaches that have developed for the sensing of oxalate and oxalic acid which shows that this is a progressing field where there are more opportunities to study the electroanalysis and expanded the use into more biological and food groups. We also compare the use of electrochemistry with that of other analytical techniques, as shown within Table 2, which shows that it is comparable in terms of their dynamic range and the limit of detection, while noting that electrochemistry has the advantages of being sensitive, selective, portable and low cost. One area that needs attention is the independent testing of electrochemical sensors need to be validated against laboratory equipment instrumentation for this field to progress further. The electrochemical sensors reported within Table 1 are prototypes which have been evaluated under traditional laboratory conditions and future challenges are to increases the minimum number of real samples to increase the pull from the commercial market to facilitate a real sensor for oxalate and oxalic acid. Further work can be directed to increase the electrochemical sensors reported within Table 1 to be combined with microfluidic techniques to allowing point-of-care sensors to be realised.

## Declaration of Competing Interest

The authors declare that they have no known competing financial interests or personal relationships that could have appeared to influence the work reported in this paper.

## Data availability

Data will be made available on request.

## References


[1] B. Hoppe, An update on primary hyperoxaluria, Nature Reviews Nephrology 8 (8) (2012) 467–475.
[2] M. Dindo, C. Conter, E. Oppici, V. Ceccarelli, L. Marinucci, B. Cellini, Molecular basis of primary hyperoxaluria: clues to innovative treatments, Urolithiasis 47 (1) (2019) 67–78.
[3] O. Efe, A. Verma, S.S. Waikar, Urinary oxalate as a potential mediator of kidney disease in diabetes mellitus and obesity, Current opinion in nephrology and hypertension 28 (4) (2019) 316–320.
[4] R. Siener, Nutrition and Kidney Stone Disease, Nutrients 13 (6) (2021) 1917.
[5] B.B. Beck, H. Hoyer-Kuhn, H. Göbel, S. Habbig, B. Hoppe, Hyperoxaluria and systemic oxalosis: an update on current therapy and future directions, Expert Opinion on Investigational Drugs 22 (1) (2013) 117–129.
[6] D. Karamad, K. Khosravi-Darani, H. Hosseini, S. Tavasoli, Analytical procedures and methods validation for oxalate content estimation, Biointerface Res Appl Chem 9 (5) (2019) 4305–4310.
[7] J. Zhi-Liang, Z. Mei-Xiu, L. Lin-Xiu, Catalytic spectrophotometric methods for the determination of oxalic acid, Analytica Chimica Acta 320 (1) (1996) 139–143.
[8] https://www.gloshospitals.nhs.uk/our-services/services-we-offer/pathology/tests-and-investigations/oxalate-urine/.
[9] B. Misiewicz, D. Mencer, W. Terzaghi, A.L. VanWert, Analytical Methods for Oxalate Quantification: The Ubiquitous Organic Anion. Molecules, Molecules 28 (2023) 3206.
[10] M.A. Zafar, Y. Liu, S. Allende, M.V. Jacob, Electrochemical sensing of oxalic acid using silver nanoparticles loaded nitrogen-doped graphene oxide, Carbon Trends 8 (2022), 100188.
[11] Y. Huang, Y.H. Zhang, Z.P. Chi, R. Huang, H. Huang, G. Liu, Y. Zhang, H. Yang, J. Lin, T. Yang, S.Z. Cao, The Handling of Oxalate in the Body and the Origin of Oxalate in Calcium Oxalate Stones, Urologia internationalis 104 (3-4) (2020) 167–176.
[12] M. Hu, G. Feng, Highly selective and sensitive fluorescent sensing of oxalate in water, Chemical Communications 48 (55) (2012) 6951–6953.
[13] S.D. Noblitt, F.M. Schwandner, S.V. Hering, J.L. Collett, C.S. Henry, High-sensitivity microchip electrophoresis determination of inorganic anions and oxalate in atmospheric aerosols with adjustable selectivity and conductivity detection, Journal of Chromatography A 1216 (9) (2009) 1503–1510.
[14] R. Liu, H. Xu, C. Xiao, H. Liu, S. Zhong, C.-H. Zeng, Preparation, luminescence and highly sensitive oxalate sensor of porous EuBO3 microwafers, Optical Materials 86 (2018) 360–365.
[15] B.G. Keevil, S. Thornton, Quantification of urinary oxalate by liquid chromatography-tandem mass spectrometry with online weak anion exchange chromatography, Clin Chem 52 (12) (2006) 2296–2299.
[16] R.L. Orwell, D.S. Scurr, A. Smith, W.G. Robertson, Measurement of oxalate in urine and urinary calculi by a new ion-chromatographic technique — a preliminary report, in: G. Gasser, W. Vahlensieck (Eds.), Pathogenese und Klinik der Harnsteine IX, Heidelberg, Steinkopff, 1982, pp. 263–270.
[17] W.J. Mayer, J.P. McCarthy, M.S. Greenberg, The determination of oxalic acid in urine by high performance liquid chromatography with electrochemical detection, Journal of chromatographic science 17 (12) (1979) 656–660.
[18] A.G. Fogg, R.M. Alonso, M.A. Fernández-Arciniega, Oxidative amperometric flow injection determination of oxalate at an electrochemically pre-treated glassy carbon electrode, Analyst 111 (2) (1986) 249–251.
[19] L.G. Shaidarova, I.A. Chelnokova, A.V. Gedmina, G.K. Budnikov, S.A. Ziganshina, A.A. Mozhanova, A.A. Bukharaev, Electrooxidation of oxalic acid at a carbon-paste electrode with deposited palladium nanoparticles, Journal of Analytical Chemistry 61 (4) (2006) 375–381.
[20] Vytřas Karel, Švancara Ivan, Metelka Radovan, Carbon paste electrodes in electroanalytical chemistry, Journal of the Serbian Chemical Society 74 (10) (2009) 1021–1033.
[21] S. Tajik, H. Beitollahi, F.G. Nejad, M. Safaei, K. Zhang, Q. Van Le, R.S. Varma, H. W. Jang, M. Shokouhimehr, Developments and applications of nanomaterial-based carbon paste electrodes, RSC Advances 10 (36) (2020) 21561–21581.
[22] I.G. Casella, Electrocatalytic oxidation of oxalic acid on palladium-based modified glassy carbon electrode in acidic medium, Electrochimica Acta 44 (19) (1999) 3353–3360.
[23] I.G. Casella, C.G. Zambonin, F. Prete, Liquid chromatography with electrocatalytic detection of oxalic acid by a palladium-based glassy carbon electrode, Journal of Chromatography A 833 (1) (1999) 75–82.
[24] L.G. Shaidarova, A.V. Gedmina, I.A. Chelnokova, G.K. Budnikov, Electrocatalytic Response of a Glassy-Carbon Electrode Modified with a Polyvinylpyridine Film with Electrodeposited Palladium in the Oxidation of Oxalic Acid, Journal of Analytical Chemistry 58 (9) (2003) 886–891.
[25] L.G. Shaidarova, S.A. Zaripova, L.N. Tikhonova, G.K. Budnikov, I.M. Fitsev, Electrocatalytic Determination of Oxalate Ions on Chemically Modified Electrodes, Russian Journal of Applied Chemistry 74 (5) (2001) 750–754.
[26] Y. Fang, X. Xu, X. Guo, B. Cui, L. Wang, Simple and ultrasensitive electrochemical sensor for oxalic acid detection in real samples by one step co-electrodeposition strategy, Analytical and Bioanalytical Chemistry 412 (23) (2020) 5719–5727.
[27] M.A.S. Amini, J.J. Vallon, Comparison of performances and analytical applications of two immobilized oxalate oxidase sensors, Analytica Chimica Acta 299 (1) (1994) 75–79.
[28] E.F. Perez, G. de Oliveira Neto, L.T. Kubota, Bi-enzymatic amperometric biosensor for oxalate, Sensors and Actuators B: Chemical 72 (1) (2001) 80–85.
[29] M.K. Sezgintürk, E. Dinçkaya, A novel amperometric biosensor based on spinach (Spinacia oleracea) tissue homogenate for urinary oxalate determination, Talanta 59 (3) (2003) 545–551.
[30] P. Vadgama, W. Sheldon, J.M. Guy, A.K. Covington, M.F. Laker, Simplified urinary oxalate determination using an enzyme electrode, Clinica Chimica Acta 142 (2) (1984) 193–201.
[31] C.S. Pundir, N. Chauhan, M. Rajneesh, Ravi Verma, A novel amperometric biosensor for oxalate determination using multi-walled carbon nanotube-gold nanoparticle composite, Sensors and Actuators B: Chemical 155 (2) (2011) 796–803.
[32] R. Mishra, H. Yadav, C.S. Pundir, An Amperometric Oxalate Biosensor Based on Sorghum Leaf Oxalate Oxidase Immobilized on Carbon Paste Electrode, Analytical Letters 43 (1) (2009) 151–160.
[33] T.E. Benavidez, R.H. Capra, C.I. Alvarez, A.M. Baruzzi, Amperometric Biosensor Based on Immobilization of Oxalate Oxidase in a Mucin/Chitosan Matrix, Electroanalysis 21 (7) (2009) 837–843.
[34] S. Milardovic, Z. Grabari $ Ac, B.S. Grabaric, Sensitive amperometric oxalate biosensor for food analysis, Food Technology and Biotechnology 38 (3) (2000) 203–210.
[35] S. Milardović, Z. Grabarić, V. Rumenjak, M. Jukić, Rapid Determination of Oxalate by an Amperometric Oxalate Oxidase-Based Electrode, Electroanalysis 12 (13) (2000) 1051–1058.
[36] M. Shan Lin, T.Feng Tseng, Chromium(III) hexacyanoferrate(II)-based chemical sensor for the cathodic determination of hydrogen peroxide, Analyst 123 (1) (1998) 159–163.
[37] S. Milardović, Z. Grabarić, M. Tkalčec, V. Rumenjak, Determination of Oxalate in Urine, Using an Amperometric Biosensor with Oxalate Oxidase Immobilized on the Surface of a Chromium Hexacyanoferrate-Modified Graphite Electrode, Journal of AOAC INTERNATIONAL 83 (5) (2019) 1212–1217.
[38] P.A. Fiorito, S.I. Córdoba de Torresi, Optimized multilayer oxalate biosensor, Talanta 62 (3) (2004) 649–654.
[39] Y. Hai, H. Yuan, D. Xiao, High electrochemiluminescence intensity of the Ru(bpy) 32+/oxalate system on a platinum net electrode, Microchimica Acta 157 (3) (2007) 127–131.
[40] I. Rubinstein, A.J. Bard, Electrogenerated chemiluminescence. 37. Aqueous ecl systems based on tris(2,2′-bipyridine)ruthenium(2+) and oxalate or organic acids, Journal of the American Chemical Society 103 (3) (1981) 512–516.
[41] N. Egashira, H. Kumasako, Y. Kurauchi, K. Ohga, Selective Determination of Oxalate with a Ruthenium(II) Complex/Nafion-Modified Electrode Combined with a Carbon Dioxide Sensor, Analytical Sciences 10 (3) (1994) 405–408.
[42] M.-H. Chiu, H. Wu, J.-C. Chen, G. Muthuraman, J.-M. Zen, Disposable Screen-Printed Carbon Electrodes for Dual Electrochemiluminescence/Amperometric

Detection: Sequential Injection Analysis of Oxalate, Electroanalysis 19 (22) (2007) 2301–2306.
[43] N. Egashira, H. Kumasako, Y. Kurauchi, K. Ohga, Determination of Oxalate in Vegetables with a Fiber-Optic Electrochemiluminescence Sensor, Analytical Sciences 8 (5) (1992) 713–714.
[44] N. Egashira, H. Kumasako, K. Ohga, Fabrication of a Fiber-Optic-Based Electrochemiluminescence Sensor and Its Application to the Determination of Oxalate, Analytical Sciences 6 (6) (1990) 903–904.
[45] L.M. Santos, R.P. Baldwin, Electrocatalytic response of cobalt phthalocyanine chemically modified electrodes toward oxalic acid and. alpha.-keto acids, Analytical chemistry 58 (4) (1986) 848–852.
[46] C. Fu, L. Wang, Y. Fang, Determination of oxalic acid in urine by co-electroosmotic capillary electrophoresis with amperometric detection, Talanta 50 (5) (1999) 953–958.
[47] B. Šljukić, R. Baron, R.G. Compton, Electrochemical Determination of Oxalate at Pyrolytic Graphite Electrodes, Electroanalysis 19 (9) (2007) 918–922.
[48] F. Wantz, C.E. Banks, R.G. Compton, Direct Oxidation of Ascorbic Acid at an Edge Plane Pyrolytic Graphite Electrode: A Comparison of the Electroanalytical Response with Other Carbon Electrodes, Electroanalysis 17 (17) (2005) 1529–1533.
[49] H. Pan, M. Wang, Y. Shen, B. Hu, Large Magneto-Current Effect in the Electrochemical Detection of Oxalate in Aqueous Solution, The Journal of Physical Chemistry C 122 (34) (2018) 19880–19885.
[50] T.A. Ivandini, T.N. Rao, A. Fujishima, Y. Einaga, Electrochemical Oxidation of Oxalic Acid at Highly Boron-Doped Diamond Electrodes, Analytical Chemistry 78 (10) (2006) 3467–3471.
[51] I.T. A. N. Yasutomo, N. Atsushi, E. Yasuaki, Gold-nanoparticle-dispersed Boron-doped Diamond Electrodes for Electrochemical Oxidation of Oxalic Acid Chemistry Letters 34 (8) (2005) 1086–1087.
[52] P. Joshi, P. Riley, K.Y. Goud, R.K. Mishra, R. Narayan, Recent advances of boron-doped diamond electrochemical sensors toward environmental applications, Current Opinion in Electrochemistry 32 (2022), 100920.
[53] T. Kondo, Y. Niwano, A. Tamura, T.A. Ivandini, Y. Einaga, D.A. Tryk, A. Fujishima, T. Kawai, Sensitive Electrochemical Detection of Oxalate at a Positively Charged Boron-Doped Diamond Surface, Electroanalysis 20 (14) (2008) 1556–1564.
[54] H. Ahmar, A.R. Fakhari, M.R. Nabid, S.J.T. Rezaei, Y. Bide, Electrocatalytic oxidation of oxalic acid on palladium nanoparticles encapsulated on polyamidoamine dendrimer-grafted multi-walled carbon nanotubes hybrid material, Sensors and Actuators B: Chemical 171-172 (2012) 611–618.
[55] R.D. Nagarajan, A.K. Sundramoorthy, One-pot electrosynthesis of silver nanorods/graphene nanocomposite using 4-sulphocalix[4]arene for selective detection of oxalic acid, Sensors and Actuators B: Chemical 301 (2019), 127132.
[56] T. Maiyalagan, P. Kannan, M. Jönsson-Niedziolka, J. Niedziolka-Jönsson, Tungsten Carbide Nanotubes Supported Platinum Nanoparticles as a Potential Sensing Platform for Oxalic Acid, Analytical Chemistry 86 (15) (2014) 7849–7857.
[57] a. Iana V.S. Arantes, Robert D. Crapnell, Elena Bernalte, Matthew J. Whittingham, Thiago R.L.C. Paixão, C.E. Banks Anal. Chem. (2023). In Press
[58] C. Kalinke, R.D. Crapnell, E. Sigley, M.J. Whittingham, P.R. de Oliveira, L. C. Brazaca, B.C. Janegitz, J.A. Bonacin, C.E. Banks, Recycled additive manufacturing feedstocks with carboxylated multi-walled carbon nanotubes toward the detection of yellow fever virus cDNA, Chemical Engineering Journal 467 (2023), 143513.
[59] M.J. Whittingham, R.D. Crapnell, E.J. Rothwell, N.J. Hurst, C.E. Banks, Additive manufacturing for electrochemical labs: An overview and tutorial note on the production of cells, electrodes and accessories, Talanta Open 4 (2021), 100051.
[60] B.C. Janegitz, R.D. Crapnell, P. Roberto de Oliveira, C. Kalinke, M.J. Whittingham, A. Garcia-Miranda Ferrari, C.E. Banks, Novel Additive Manufactured Multielectrode Electrochemical Cell with Honeycomb Inspired Design for the Detection of Methyl Parathion in Honey Samples, ACS Measurement Science Au 3 (3) (2023) 217–225.
[61] S. Hussain, S. Abbas Zaidi, D. Vikraman, H.-S. Kim, J. Jung, Facile preparation of tungsten carbide nanoparticles for an efficient oxalic acid sensor via imprinting, Microchemical Journal 159 (2020), 105404.
[62] R.D. Crapnell, N.C. Dempsey-Hibbert, M. Peeters, A. Tridente, C.E. Banks, Molecularly imprinted polymer based electrochemical biosensors: Overcoming the challenges of detecting vital biomarkers and speeding up diagnosis, Talanta Open 2 (2020), 100018.
[63] X. Luo, L. Chen, J. Yang, S. Li, M. Li, Q. Mo, Y. Li, X. Li, Electrochemically simultaneous detection of ascorbic acid, sulfite and oxalic acid on Pt-Pd nanoparticles/chitosan/nitrogen doped graphene modified glassy carbon electrode: A method for drug quality control, Microchemical Journal 169 (2021), 106623.
[64] L.V. Souza, A.H. Virgili, G.O. Teixeira, R. Hinrichs, D. Bianchini, T.M.H. Costa, L. T. Arenas, E.V. Benvenutti, E.W. de Menezes, Mesoporous structured silica modified with niobium oxide and cobalt hematoporphyrin applied to the simultaneous electrochemical evaluation of oxalic and uric acids, Journal of Sol-Gel Science and Technology 102 (1) (2022) 18–29.
[65] Y. Liu, J. Huang, D. Wang, H. Hou, T. You, Electrochemical determination of oxalic acid using palladium nanoparticle-loaded carbon nanofiber modified electrode, Analytical Methods 2 (7) (2010) 855–859.
[66] F. Manea, C. Radovan, I. Corb, A. Pop, G. Burtica, P. Malchev, S. Picken, J. Schoonman, Simultaneous Determination of 4-Chlorophenol and Oxalic Acid Using an Expanded Graphite-Epoxy Composite Electrode, Electroanalysis 20 (15) (2008) 1719–1722.
[67] P.A. Fiorito, S.I. Córdoba de Torresi, Hybrid nickel hexacyanoferrate/polypyrrole composite as mediator for hydrogen peroxide detection and its application in oxidase-based biosensors, Journal of Electroanalytical Chemistry 581 (1) (2005) 31–37.
[68] S. Yadav, R. Devi, S. Kumari, S. Yadav, C.S. Pundir, An amperometric oxalate biosensor based on sorghum oxalate oxidase bound carboxylated multiwalled carbon nanotubes–polyaniline composite film, Journal of Biotechnology 151 (2) (2011) 212–217.
[69] R.H. Capra, M. Strumia, P.M. Vadgama, A.M. Baruzzi, Mucin/carbopol matrix to immobilize oxalate oxidase in a urine oxalate amperometric biosensor, Analytica Chimica Acta 530 (1) (2005) 49–54.
[70] R. Devi, S. Relhan, C.S. Pundir, Construction of a chitosan/polyaniline/graphene oxide nanoparticles/polypyrrole/Au electrode for amperometric determination of urinary/plasma oxalate, Sensors and Actuators B: Chemical 186 (2013) 17–26.
[71] F. Manea, C. Radovan, I. Corb, A. Pop, G. Burtica, P. Malchev, S. Picken, J. Schoonman, Electrochemical Oxidation and Determination of Oxalic Acid at an Exfoliated Graphite-Polystyrene Composite Electrode, Sensors 7 (4) (2007) 615–627.
[72] S.-i. Yamazaki, N. Fujiwara, K. Yasuda, A catalyst that uses a rhodium phthalocyanin for oxalic acid oxidation and its application to an oxalic acid sensor, Electrochimica Acta 55 (3) (2010) 753–758.
[73] T. Alizadeh, S. Nayeri, N. Hamidi, Graphitic carbon nitride (g-C3N4)/graphite nanocomposite as an extraordinarily sensitive sensor for sub-micromolar detection of oxalic acid in biological samples, RSC Advances 9 (23) (2019) 13096–13103.
[74] X. Chen, Z. Cai, Z. Huang, M. Oyama, Y. Jiang, X. Chen, Non-enzymatic oxalic acid sensor using platinum nanoparticles modified on graphene nanosheets, Nanoscale 5 (13) (2013) 5779–5783.
[75] T. Dodevska, I. Shterev, Electrochemical non-enzymatic sensing of oxalic acid based on PdPt-modified electrodes: application to the analysis of vegetable samples, Monatshefte für Chemie - Chemical Monthly 151 (4) (2020) 495–504.
[76] Y. Zheng, C. Yang, W. Pu, J. Zhang, Determination of oxalic acid in spinach with carbon nanotubes-modified electrode, Food Chemistry 114 (4) (2009) 1523–1528.
[77] K. Income, N. Ratnarathorn, S. Themsirimongkon, W. Dungchai, An Oxalic Acid Sensor Based on Platinum/Carbon Black-Nickel-Reduced Graphene Oxide Nanocomposites Modified Screen-Printed Carbon Electrode, J. Electrochem. Sci. Technol 10 (4) (2019) 416–423.
[78] B.G. Keevil, S. Thornton, Quantification of Urinary Oxalate by Liquid Chromatography–Tandem Mass Spectrometry with Online Weak Anion Exchange Chromatography, Clinical chemistry 52 (12) (2006) 2296–2299.
[79] H. Khajehsharifi, A. Hemmati Yadkury, A. Shokrollahi, M. Bordbar, Naked Eye Chemosensor for the Qualitative and Quantitative Determination of Oxalate Ions Based on Indicator Displacement Assay, Analytical and Bioanalytical Chemistry Research 7 (1) (2020) 111–129.
[80] Y. Gan, N. Hu, C. He, S. Zhou, J. Tu, T. Liang, Y. Pan, D. Kirsanov, A. Legin, H. Wan, P. Wang, MnO2 nanosheets as the biomimetic oxidase for rapid and sensitive oxalate detection combining with bionic E-eye, Biosensors and Bioelectronics 130 (2019) 254–261.
[81] K. Hu, X. Chen, X. Song, Y. Wu, K. Huang, P. Chen, Carbon dots and MnO2 nanosheet nanocomposites sensing platform for sensitive detection of oxalate in urine samples of urolithiasis patients, Talanta 266 (2024), 124976.
[82] S.D. Noblitt, F.M. Schwandner, S.V. Hering, J.L. Collett Jr., C.S. Henry, High-sensitivity microchip electrophoresis determination of inorganic anions and oxalate in atmospheric aerosols with adjustable selectivity and conductivity detection, Journal of chromatography. A 1216 (9) (2009) 1503–1510.